


NANO EXPRESS

Open Access



Defect and Doping Engineered Penta-graphene for Catalysis of Hydrogen Evolution Reaction

Jinbo Hao¹, Feng Wei², Xinhui Zhang^{1*} , Long Li¹, Chunling Zhang¹, Dan Liang^{2*}, Xiaoguang Ma³ and Pengfei Lu^{1,2}

Abstract

Water electrolysis is a sustainable and clean method to produce hydrogen fuel via hydrogen evolution reaction (HER). Using stable, effective and low-cost electrocatalysts for HER to substitute expensive noble metals is highly desired. In this paper, by using first-principles calculation, we designed a defect and N-, S-, P-doped penta-graphene (PG) as a two-dimensional (2D) electrocatalyst for HER, and its stability, electronic properties and catalytic performance were investigated. The Gibbs free energy (ΔG_{H}), which is the best descriptor for the HER, is calculated and optimized, the calculation results show that the ΔG_{H} can be 0 eV with C2 vacancies and P doping at C1 active sites, which should be the optimal performance for a HER catalyst. Moreover, we reveal that the larger charge transfer from PG to H, the closer ΔG_{H} is to zero according to the calculation of the electron charge density differences and Bader charges analysis. Ulteriorly, we demonstrated that the HER performance prefers the Volmer–Heyrovsky mechanism in this study.

Keywords: Penta-graphene, Hydrogen evolution reaction, Electrocatalysis, First-principles calculation

Background

Because of the climate change and environmental pollution caused by fossil fuels usage, exploitation and utilization of clean and renewable energy are the mean way after nowadays [1–4]. As a clean, renewable and environmentally friendly energy source, hydrogen (H_2) has been attracting considerable attention to fulfill human future energy needs [5, 6]. Water electrolysis is a sustainable and clean method to produce H_2 , and electrocatalysts can enhance the efficiency of water splitting observably [7, 8]. For hydrogen evolution reaction (HER), platinum-based nanomaterials are considered as the best electrocatalysts because of a small Tafel slope, a low overpotential,

a slightly negative Gibbs free energy (ΔG_{H}) and a high exchange current density [9, 10], but the scarcity and high cost hamper their industrial scale applications [11]. Therefore, developing effective, earth-abundant and low-cost electrocatalysts is essential for HER [12–14].

In fact, a wide range of earth-abundant electrocatalysts have been studied and designed for HER [15–17]. Among these materials, two-dimensional (2D) nanomaterials provide new opportunities for HER because of the compelling structural and electronic properties. To date, the transition metal dichalcogenides (TMDs) and the graphene-based materials are the biggest and most intensively studied groups of 2D electrocatalysts for HER [18–23]. The TMDs HER catalysts have low overpotential and small Tafel slope, unusual electronic properties and high air stability, exhibit high HER performance, and different methods were taken for enhancing their catalytic performance [24, 25]. The graphene-based HER catalysts have attracted considerable attention and persistent studying because of their

*Correspondence: zhangxinhui@xauat.edu.cn; liangdan@bupt.edu.cn

¹ School of Science, Xi'an University of Architecture and Technology, Xi'an 710055, China

² State Key Laboratory of Information Photonics and Optical Communications, Beijing University of Posts and Telecommunications, Beijing 100876, China

Full list of author information is available at the end of the article

distinctive structural merits, such as high electrical conductivity, large surface area and good chemical stability [26, 27]. Many methods were taken for enhancing the catalytic activity, such as heteroatom doping and deflection engineering [28, 29]. Meanwhile, the intensive research on other new 2D carbon allotropes have also been developed, such as graphdiyne [30] and penta-graphene (PG) [31]. As a 2D carbon allotrope, PG is composed of only carbon pentagons and inherits many exceptional properties of 2D materials, such as finite electronic band gap, abundant active sites and large surface area, so it is anticipated to be a versatile material for lots of potential applications like other 2D graphene-based materials [32–35]. Since there are only applications in gas adsorption [36–38], H₂ storage [39, 40], anode materials at present [41, 42], no report has ever been found on the application in HER. Therefore, research on HER by PG is of great significance and cannot only fill such a gap but also broaden the scope of graphene-based HER catalysts. However, the pristine PG is found to be inert for the HER with a relatively large ΔG_{H} , which means that hydrogen adsorption is difficult and inhibits the HER. This is similar to the problems encountered by pristine graphene ($\Delta G_{\text{H}} = 1.85$ eV [43]). Heteroatom doping into graphene-based materials could adjust their electronic and catalytic properties, which makes them prospective catalysts for the practical applications [3]. Therefore, we managed to tailor the catalytic activity of PG by heteroatom doping [44–46] and deflection engineering [47, 48].

In this paper, by using first-principles calculation, we designed and demonstrated a defect and N-, S-, P-doped PG and investigated their stability and electronic properties and evaluated their performance as HER electrocatalysts. Our results reveal that the defect and doped PG can obviously enhance the catalytic activity toward HER, compared with the pristine PG. It is also shown that the ΔG_{H} can be 0 eV with C2 vacancies and P doping at C1 active sites, which should be the optimal performance for a HER catalyst, so P-doped PG has the optimal ΔG_{H} and activation energy barrier for the rate-determining step among the three counterparts, and it exhibits more favorable performance. We further show that the catalytic activity arises from the incorporated doping atoms, which can provide efficient pathway for charge transport during the electrolysis, resulting in the reduction in ΔG_{H} . We also demonstrate that the Volmer–Heyrovsky mechanism is more preferred for HER on defect and doped PG. We compared our results with that of other researchers on graphene, and it can be found that the deflection and doping engineering are more effective for PG in catalysis of HER. Thus, our effort on defect and doped PG makes

it a high promising electrocatalyst for HER, and our findings provide a deep understanding in designing efficient and durable electrocatalysts. This method can be also applied to other graphene-based materials.

Computational Methods

Our first-principles calculations were performed using the Vienna Ab initio Simulation Package (VASP) [49]. The projected augmented wave (PAW) potentials were used to analyze the interactions between core electrons and valence electrons [50–52]. The electron exchange–correlation interactions were described by using the Perdew–Burke–Ernzerhof (PBE) functional within the generalized gradient approximation (GGA) [53]. The DFT-D3 exchange–correlation functional was introduced in structural optimization to take the van der Waals interaction into account. The vacuum space along the *z*-direction was set to 20 Å in order to eliminate the interactions between PG and its periodic images.

The plane-wave energy cutoff was set to be 500 eV. The convergence criterion was set as 10^{−5} eV for a total energy. All the atomic positions and lattice structures were fully relaxed with the threshold of a maximum force of 0.02 eV Å^{−1}. In order to ensure the accuracy and efficiency of the calculation, a Gamma-centered k-point mesh with a Monkhorst–Pack method 5 × 5 × 1 was employed for all considered structures after convergence test [54]. The amount of the charge transfer between the C atoms and H atoms was calculated using Bader code [55]. We also calculated H* adsorption energy barriers using the climbing image-nudged elastic band (CI-NEB) method [56, 57]. The CI-NEB is an efficient method to determine the minimum energy path and saddle points between a given initial and final position [58–60], and in our CI-NEB calculations, the initial and the final structures were fully optimized.

The adsorption energy (ΔE_{H}) is defined as

$$\Delta E_{\text{H}} = E(*\text{H}) - E(*) - \frac{1}{2}E(\text{H}_2)$$

where $E(*\text{H})$ and $E(*)$ are the total energy of structures with and without hydrogen adsorption, respectively, and $E(\text{H}_2)$ is the total energy of a H₂ molecule.

The Gibbs free energy (ΔG_{H}) is defined as:

$$\Delta G_{\text{H}} = \Delta E_{\text{H}} + \Delta E_{\text{ZPE}} - T\Delta S_{\text{H}}$$

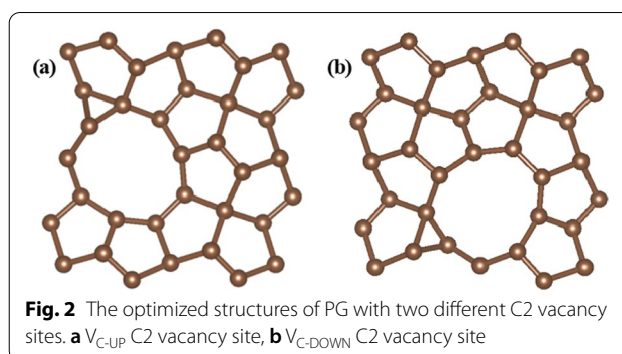
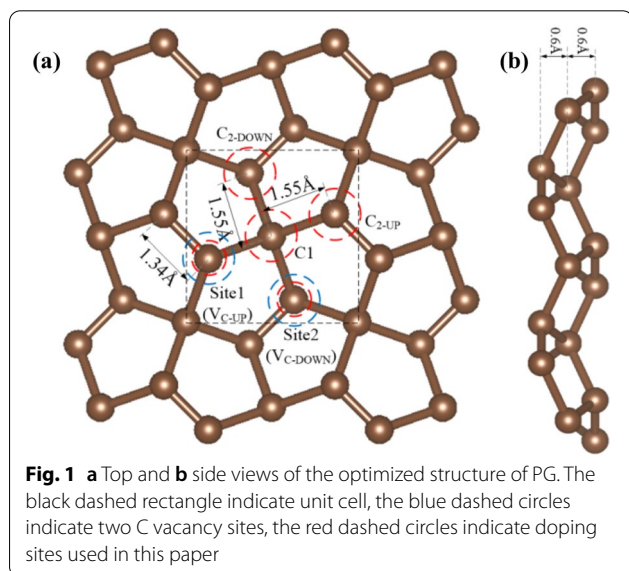
where ΔE_{H} is the adsorption energy, ΔE_{ZPE} is the difference in zero-point energy, T is the temperature (298.15 K) and ΔS_{H} is the entropy difference of H adsorbed and H in the gas phase. We approximated the entropy of hydrogen adsorption as $\Delta S_{\text{H}} \approx \frac{1}{2}(S_{\text{H}_2}^{\circ})$, where $S_{\text{H}_2}^{\circ}$ is the entropy of gas phase H₂ at standard conditions, $T\Delta S_{\text{H}}$ was set to be −0.202 eV after calculation in this study.

Results and Discussion

Structure and Catalytic Activity of Defect and Doped PG

The optimized structure of PG is shown in Fig. 1. For convenience of discussion, we hereafter group the sp^3 - and sp^2 - hybridized C atoms as C1 and C2, respectively. The distance between the C1 and C2 is 1.55 Å, and the C2–C2 bond length is 1.34 Å, which is consistent with the experimental result [31].

At the beginning, we first investigated the sites C1 and C2 in the basal plane of pristine PG for HER, the calculated ΔG_H values are 2.43 eV and 2.72 eV, respectively. So our calculations show that the pristine PG is found to be inert for the HER with a relatively large ΔG_H of H, which means that hydrogen adsorption is difficult and HER is inhibited. Therefore, we managed to use some methods to tailor the catalytic activity of PG. We researched the possible active sites for doping and we also investigated the active sites for C1 and C2 with N, S, P doping, respectively. The calculation results show that no obvious improvement of HER can be obtained if only doping engineering was introduced. In the case of the P-doped structure, the calculated ΔG_H values of C1 and C2 sites are 1.24 eV and 1.40 eV, respectively. Ulteriorly, we investigated the defect PG with C vacancy sites. The calculation results reveal that C1 vacancy structure cannot improve the HER performance but C2 vacancy structure can decrease ΔG_H obviously, so we use C2 vacancy structure in this study. The optimized structures with V_{C-UP} and V_{C-DOWN} C2 vacancies sites are shown in Fig. 2, the vacancy defects are built by removing C2 atoms from C_{2-UP} or C_{2-DOWN} site in a 24-atom supercell. The calculated ΔG_H values are shown in Table 1, where C1 and C2 are the active sites for hydrogen adsorption.



Though it is confirmed by our calculations that C2 vacancies are efficient to enhance the HER activity, PG with C2 vacancy structure is not yet optimal for a HER catalyst. Thus, we further investigated the defect and doped PG for HER. We used PG with C2 vacancy as initial structure, which is shown in Fig. 2 and then investigated all the different possible active sites with N, S, P doping, including C1, C_{2-UP} and C_{2-DOWN} sites. As a result, we found that better HER performance could be achieved with a combination of C2 vacancy and heteroatom doping. We investigated all the possible structures, and the results showed that there are two structures that can achieve better HER performance, one structure is a combination of the C_{2-UP} vacancy and heteroatom doping in the C_{2-DOWN} site, and the other is a combination of the C_{2-DOWN} vacancy and heteroatom doping in the C_{2-UP} site. So we focused on these two structures and found that they can shift the ΔG_H values closer to zero. The optimized structures are shown in Fig. 3, and the calculated bond lengths are summarized in Table 2.

We can see that there is slight difference between the corresponding bond lengths of N-doped PG and that

Table 1 Calculated ΔG_H values for different possible active sites

Structure	Site	ΔG_H (eV)
Pristine	C1	2.43
	C2	2.72
N-doped	C1	1.48
	C2	1.99
S-doped	C1	1.53
	C2	1.65
P-doped	C1	1.24
	C2	1.40
V_{C-UP}	C1	0.24
	C2	0.25
V_{C-DOWN}	C1	0.23
	C2	0.24

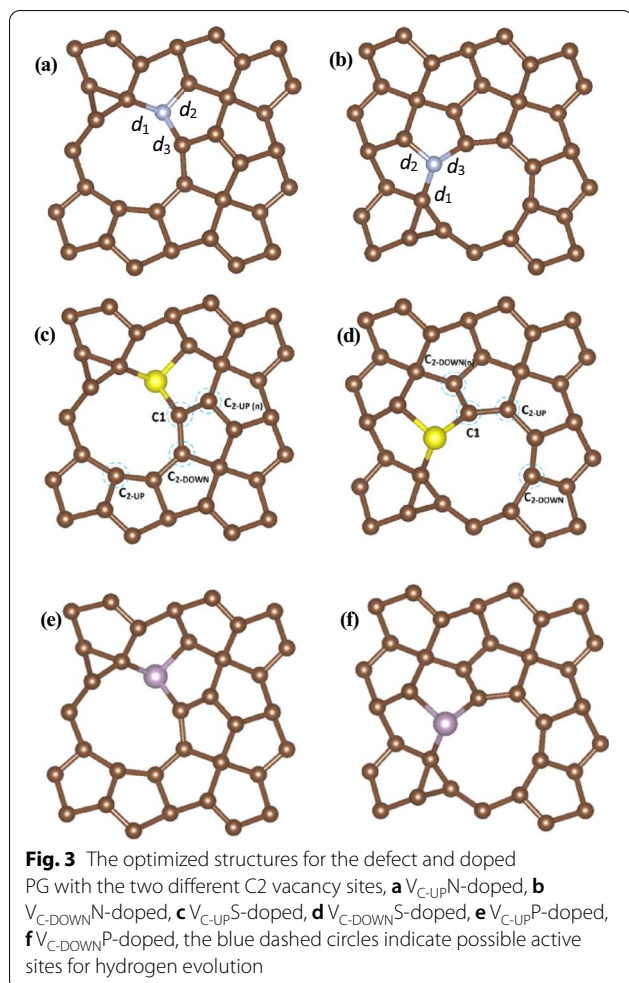


Table 2 Calculated bond lengths of C2 vacancy and N-, S-, P-doped PG

Structure	d_1 (Å)	d_2 (Å)	d_3 (Å)
V_{C-UP} N-doped	1.50	1.39	1.42
V_{C-UP} S-doped	1.95	1.79	1.73
V_{C-UP} P-doped	1.89	1.81	1.79
V_{C-DOWN} N-doped	1.51	1.39	1.42
V_{C-DOWN} S-doped	1.95	1.80	1.74
V_{C-DOWN} P-doped	1.89	1.81	1.80

of pristine PG. Because of the large radius of S and P atoms, these two structures undergo much more distortion, but they can both maintain the structure of PG.

To investigate the stability of PG with C2 vacancy and heteroatom doping, we calculated the formation energy, which is defined as

$$E_f = \left(E_t - E_V + E_C - E_d - \frac{1}{2}\mu_H \right)$$

where E_t is the total energy of the defect and doped system, and E_V is the energy of C2 vacancy PG, E_C is the average energy per C atom of the pristine PG, E_d is the energy of doping atoms, μ_H is taken from the total energy of the H_2 molecule, respectively. One of our calculation results about the formation energies of preceding two structures with C1 active sites for HER is shown in Fig. 4. We can see that negative formation energies indicate energetically favorable and feasible defect and S-, P-doped PG. Similarly, E_f values of N-doped structures with active sites for HER are all positive. We investigated all the possible active sites and got the similar results as shown in Fig. 4, so we will investigate only the S- and P-doped PG. According to the definition, a more negative E_f value indicates higher stability of the structure, so P-doped PG has excellent stability, as well as good HER performance.

Origin of the HER Catalytic Activity DOS and Band Structures

To achieve an in-depth understanding of the nature of C2 vacancy and doping engineering in the HER activity, we investigated the total and projected DOS, electronic band structure of the defect and S-, P-doped PG. Figure 5 is one of our calculation results about electronic band structures, total and projected DOS of pristine PG, V_{C-UP} , V_{C-UP} S-doped and V_{C-UP} P-doped PG.

From the figure, we can see that when C2 vacancy is introduced, some new defect states highlighted by red curves appear in the forbidden band near the Fermi level. Obviously, these new states arise from the C2 vacancy. Furthermore, when S, P heteroatom doping is

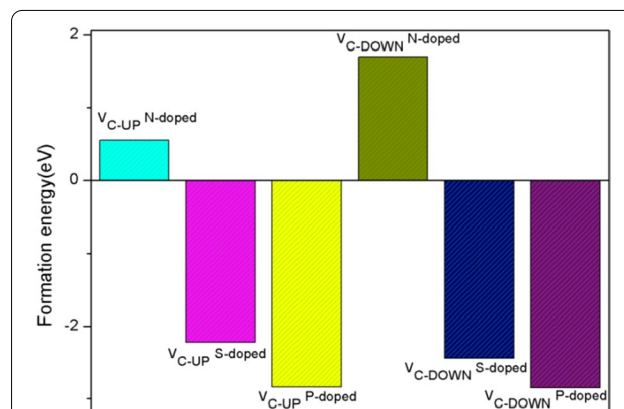
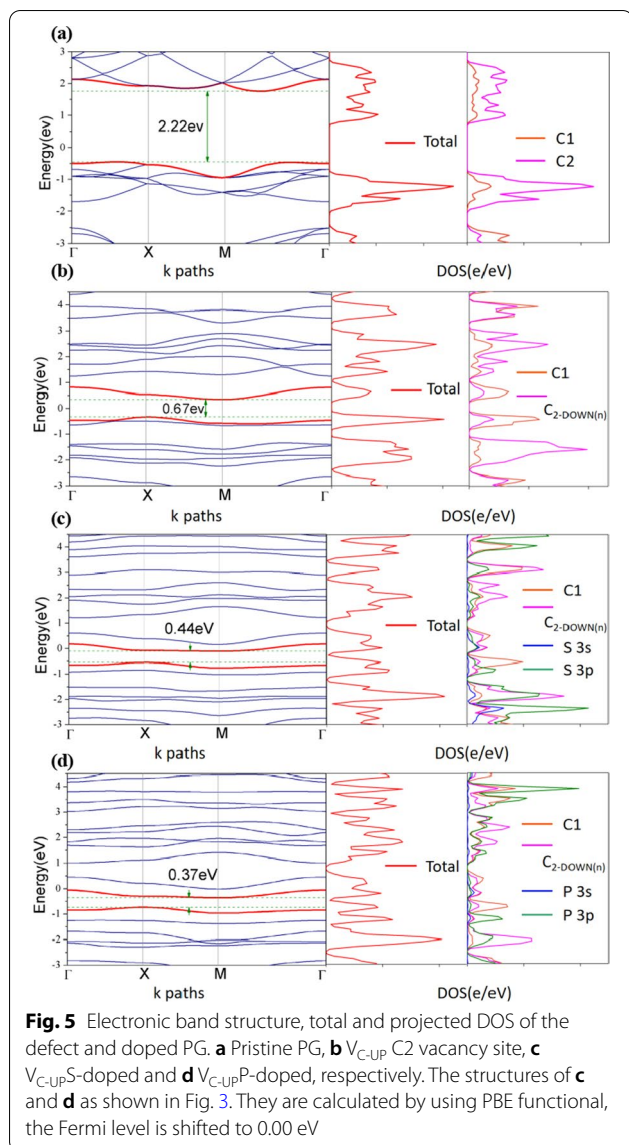
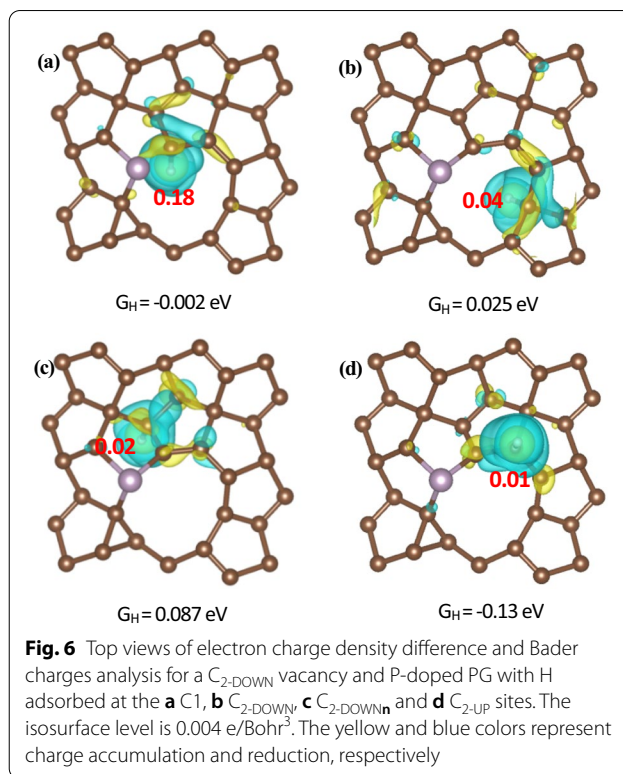


Fig. 4 Formation energy of two initial defect and doped PG structures with C1 active sites for HER, more negative value indicates higher stability of the structure



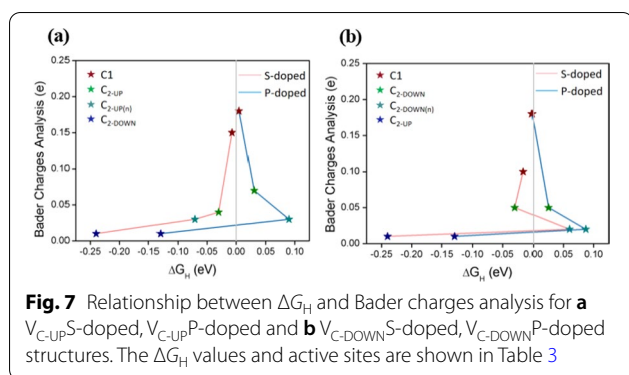
introduced, the band gap gets narrower (from 2.22 eV [31] to 0.37 eV) and the number of new defect states near the Fermi level increases, which can possibly improve the H^* adsorption strength.

However, we found that the DOS of V_{C-UP} near the Fermi level is much larger than that of pristine PG. In addition, the electron density near the Fermi level of C2 vacancy and S-, P-doped PG is further increased relative to pristine PG. We also found that the S 3p and P 3p orbitals undergo significant hybridization with the C1 and C2 states, leading to strong interactions between the heteroatoms and C, and the formation of S–C and P–C bonds. These results demonstrate that combination of the C2 vacancy and S, P heteroatoms doping may be a better engineering for improving HER activity.



Electron Density Difference and Charge Transfer

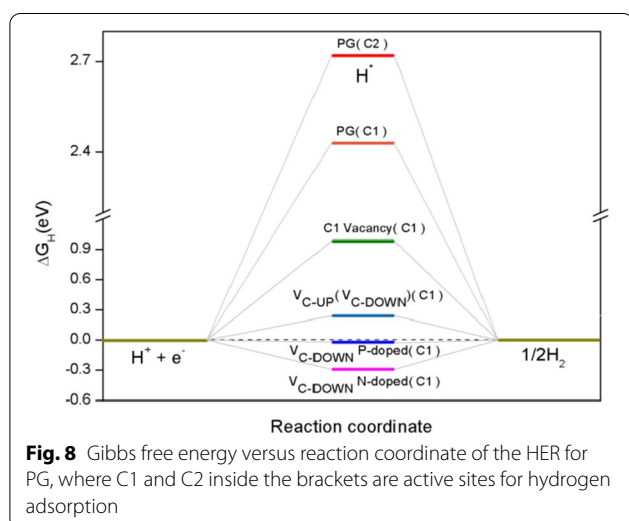
Moreover, to study the binding interaction between the H atom and PG, we calculated the electron charge density differences for defect and S-, P-doped PG with different active sites for hydrogen evolution. One of our calculation results about the electron charge density difference and Bader charges analysis for a C_{2-DOWN} vacancy and P-doped PG with H^* adsorbed at the different active sites for hydrogen adsorption is shown in Fig. 6. The yellow and blue colors represent charge accumulation and reduction, respectively. It is shown that the electrons accumulate around H atoms and reduce around the C atoms which are bonded to H atoms, indicating a charge transfer from PG to H^* . The charge transfer is also confirmed by Bader charges analysis. The calculation results show that there are 0.18, 0.04, 0.02 and 0.01 electrons transferring to H^* at C1, C_{2-DOWN} , $C_{2-DOWN(n)}$ and C_{2-UP} sites, respectively. We further show that the larger charge transfer from PG to H^* , the closer ΔG_H is to zero, which means the optimal performance for a HER catalyst, as shown in Fig. 7. It can be seen from Fig. 6 that electrons are transferred from PG to H^* , resulting in increase in the charge density of the bonds, which means that the stabilization of the H^* species in HER performance may originate from the enhanced charge density of P-doped C atoms, indicating that P atoms are inherently advantageous in interacting with H atoms than C atoms. We also



noticed that H^* is absorbed onto C instead of P, indicating that the increased charge density can contribute to the electrocatalyst on H atom. So our calculations show that P doping into the PG can lead to enhanced adsorption of H^* on C atoms. As mentioned above, the DFT calculations also suggested that the P doping into PG could much more efficiently enhance the HER activity than that of S-doping.

Activity of Defect and Doped PG Toward HER Gibbs Free Energies of HER

The ΔG_H is the vital descriptor of the HER for a variety of electrocatalysts, the optimal ΔG_H value for a electrocatalyst is zero, so the H^* adsorption and desorption can occur spontaneously without activation energy barrier [61, 62]. To evaluate the HER activity of the PG and investigate the deflection and doping engineering, we calculated the ΔG_H of HER. One of our calculation results about ΔG_H versus reaction coordinate of the HER for PG is shown in Fig. 8, where C1 and C2 inside the brackets are active sites for hydrogen adsorption.



Our calculations show that the pristine PG is found to be inert for the HER with a relatively large Gibbs free energy of H^* ($\Delta G_H = 2.72$ eV(C2), $\Delta G_H = 2.43$ eV(C1)). When vacancies are introduced, there are two different C vacancy sites, C1 vacancy site and C2 vacancy site. We calculated the ΔG_H on the two sites and found that C2 vacancy can notably decrease ΔG_H ($\Delta G_H = 0.24$ eV), which indicates that H^* preferentially adsorbs on C2 vacancy structures. The optimized structures with C2 vacancy sites (V_{C-UP} and V_{C-DOWN}) are shown in Fig. 2. Though C2 vacancies show significant improvement over the pristine PG, they are still not the optimal for the hydrogen adsorption, so doping engineering is explored to improve the HER performance. We show our effects of C2 vacancies and S, P heteroatom doping on the HER activity and optimize the HER performance. The ΔG_H values are summarized in Table 3, and the active sites for hydrogen evolution are shown in Fig. 3.

The calculation results reveal that ΔG_H decreases significantly, demonstrating that the deflection and doping engineering are very effective in reducing ΔG_H . Remarkably, we found that the ΔG_H values of active sites C1, C_{2-UP} and $C_{2-UP(n)}$ for V_{C-UP} , active sites C1, C_{2-DOWN} and $C_{2-DOWN(n)}$ for V_{C-DOWN} are very close to zero, especially for two C1 sites, signifying the optimal conditions can be achieved, which are significantly superior to pristine PG. And we compared our results with previous work from other researchers on graphene, for instance, graphene with C vacancy ($\Delta G_H = -2.108$ eV) [28], graphene with N-doped ($\Delta G_H = -0.693$ eV) [28], graphene with C vacancy and N-doped ($\Delta G_H = -0.595$ eV) [28], graphene

Table 3 Calculated ΔG_H values of C2 vacancies and S-, P-doped PG

Structure	Site	ΔG_H (eV)
V_{C-UP} S-doped	C1	-0.007
	C_{2-UP}	-0.030
	$C_{2-UP(n)}$	-0.071
	C_{2-DOWN}	-0.240
V_{C-UP} P-doped	C1	0.005
	C_{2-UP}	0.030
	$C_{2-UP(n)}$	0.090
	C_{2-DOWN}	-0.130
V_{C-DOWN} S-doped	C1	-0.016
	C_{2-DOWN}	-0.030
	$C_{2-DOWN(n)}$	0.060
	C_{2-UP}	-0.240
V_{C-DOWN} P-doped	C1	-0.002
	C_{2-DOWN}	0.025
	$C_{2-DOWN(n)}$	0.087
	C_{2-UP}	-0.130

with S-doped ($\Delta G_{\text{H}} = -0.30$ eV) [29] and graphene with N/S co-doped ($\Delta G_{\text{H}} = -0.12$ eV) [29]. We can find that the defection and doping engineering are more effective for PG. Thus, our results clearly suggest that the ΔG_{H} of PG can be manipulated by applying defection and doping engineering to achieve the optimal HER activity.

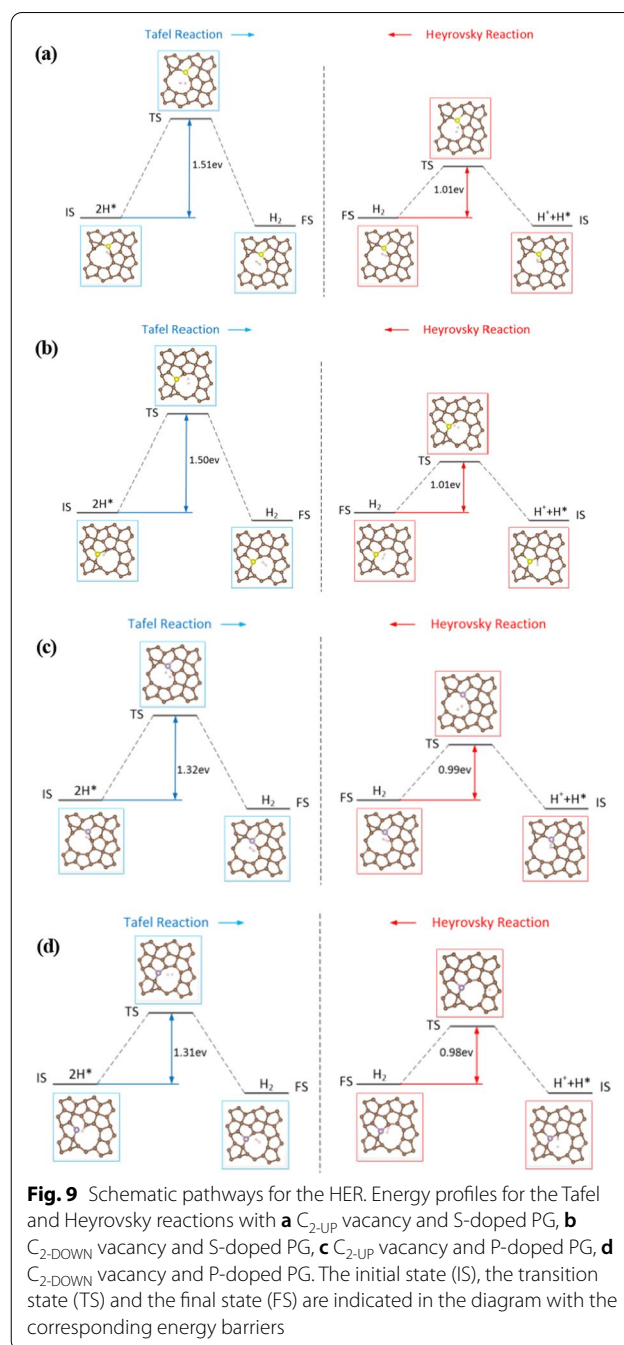
The Reaction Pathways of Defect and Doped PG

The HER proceeds in a multistep electrochemical process, via one of two pathways which are known as the Volmer–Tafel and the Volmer–Heyrovsky mechanisms. The first step of HER is the H^* adsorption on the electrocatalyst surface (i.e., Volmer reaction), which is described by $\text{H}^+ + \text{e}^- \rightarrow \text{H}^*$. Then, H^* combines with H^+ and an electron (e^-) to form a H_2 molecule, known as the Heyrovsky step, which is described by $\text{H}^* + \text{H}^+ + \text{e}^- \rightarrow \text{H}_2$. Alternatively, H_2 molecule can be formed via the Tafel step, i.e., the combination of two H^* on the electrocatalyst surface, which is described by $2\text{H}^* \rightarrow \text{H}_2$ [63].

To investigate the defection and doping engineering effects on PG and further understand the mechanism of superior HER activity, the energy barriers of Tafel and Heyrovsky reactions with $\text{C}_{2\text{-UP}}$ and $\text{C}_{2\text{-DOWN}}$ vacancies, S-, P-doped PG for C1 site were calculated. The initial state (IS), the final state (FS) and the transition state (TS) are displayed in Fig. 9 with the corresponding energy barriers. For the Tafel reaction, the recombination of 2H^* shows energy barriers of 1.51 eV (S-doped), 1.32 eV (P-doped), respectively. Whereas the release of a H_2 molecule in the Heyrovsky reaction involved in a proton reacting with an adsorbed H^* needs to overcome the energy barriers of 1.01 eV (S-doped), 0.99 eV (P-doped), respectively. The results reveal that the energy barriers of Tafel reaction are significantly higher than that of the Heyrovsky reaction. So the HER on defect and doped PG prefers the Volmer–Heyrovsky mechanism.

Conclusions

We theoretically designed a C vacancy and N-, S-, P-doped PG and investigated their stability and unique role of electrocatalyst toward HER systematically. We find that defection and doping engineering possess a superior HER performance over the pristine PG. Importantly, the optimal HER activity can be achieved with C2 vacancies and S, P heteroatoms doping, which indicates that the catalytic properties of the defect and doped PG can be tuned easily and effectively. Our calculations reveal that ΔG_{H} decreases significantly with C2 vacancies and S, P heteroatom doping, and the optimal conditions can be achieved with P doping at C1 active sites, for which defection or doping engineering alone cannot achieve the optimal conditions. The electronic structure analysis shows that when C2 vacancy



and S, P heteroatom doping are introduced, several new defection states move closer to the Fermi level, leading to the narrower band gap and an improvement of the hydrogen adsorption strength. We also find the charge transfer from PG to H^* by calculating the electron charge density differences, the larger charge transfer to H^* , the closer ΔG_{H} values to zero by using Bader charges analysis, which indicates the optimal performance for a HER catalyst. And we further demonstrate

the HER on defect and doped PG prefers the Volmer–Heyrovsky mechanism. So our study shows that the designed defect and doped PG is highly activated toward HER electrocatalyst, the optimal HER activity can be achieved, and abundant catalytic activity sites are provided. It is expected that the strategies developed in this paper may be applied for designing 2D graphene-based electrocatalysts for low-cost and high-performance HER applications.

Abbreviations

HER: Hydrogen evolution reaction; PG: Penta-graphene; 2D: Two dimensional; ΔG_{\ddagger} : The Gibbs free energy; TMDs: The transition metal dichalcogenides; VASP: Vienna Ab initio Simulation Package; PAW: Projected augmented wave; PBE: The Perdew–Burke–Ernzerhof; GGA: The generalized gradient approximation; CI-NEB: The climbing image-nudged elastic band; IS: Initial state; FS: The final state; TS: The transition state.

Authors' contributions

XHZ and DL conceived and designed the study. JBH, FW and LL performed the calculations and analyzed the result data; JBH and CLZ wrote the manuscript, XGM and PFL participated in the discussions and edited the manuscript. All authors read and approved the final manuscript.

Funding

This work was supported by the Fund of State Key Laboratory of IPOC (BUPT) (IPOC2019ZZ04 and IPOC2019A013), and the Open-Foundation of Key Laboratory of Laser Device Technology, China North Industries Group Corporation Limited (No. KLLDT202001).

Availability of data and materials

The datasets supporting the conclusions of this article are included within the article, and further information about the data and materials could be made available to the interested party under a motivated request addressed to the corresponding author.

Declarations

Competing interests

The authors declare that they have no competing interests.

Author details

¹School of Science, Xi'an University of Architecture and Technology, Xi'an 710055, China. ²State Key Laboratory of Information Photonics and Optical Communications, Beijing University of Posts and Telecommunications, Beijing 100876, China. ³School of Physics and Optoelectronic Engineering, Ludong University, Yantai 264025, China.

Received: 24 May 2021 Accepted: 5 August 2021

Published online: 13 August 2021

References

- Chu S, Majumdar A (2012) Opportunities and challenges for a sustainable energy future. *Nature* 488:294–303
- Hu GX, Fung V, Sang XH, Unocic RR, Ganesh P (2019) Superior electrocatalytic hydrogen evolution at engineered non-stoichiometric two-dimensional transition metal dichalcogenide edges. *J Mater Chem A* 7:18357–18364
- Ren CJ, Wen L, Magagula S, Jiang QY, Lin W, Zhang YF, Chen ZF, Ding KN (2020) Relative efficacy of Co- X_4 embedded grapheme ($X=N, S, B$, and P) electrocatalysts towards hydrogen evolution reaction: is nitrogen really the best choice? *ChemCatChem* 12:536–543
- Liang D, Zhang YW, Lu PF, Yu ZG (2019) Strain and defect engineered monolayer Ni-MoS₂ for pH-universal hydrogen evolution catalysis. *Nanoscale* 11:18329–18337
- Korotcenkov G, Han SD, Stetter JR (2009) Review of electrochemical hydrogen sensors. *Chem Rev* 109:1402–1433
- Geng XM, Sun WW, Wu W, Chen B, Al-Hilo A, Benamara M, Zhu HL, Watanabe F, Cui JB, Chen TP (2016) Pure and stable metallic phase molybdenum disulfide nanosheets for hydrogen evolution reaction. *Nat Commun* 7:10672
- Zhou YC, Leng YH, Zhou WJ, Huang JL, Zhao MW, Zhan J, Feng CH, Tang ZH, Chen SW, Liu H (2015) Sulfur and nitrogen self-doped carbon nanosheets derived from peanut root nodules as high-efficiency non-metal electrocatalyst for hydrogen evolution reaction. *Nano Energy* 16:357–366
- Li Y, Wei XF, Chen LS, Shi JL, He MY (2019) Nickel-molybdenum nitride nanoplate electrocatalysts for concurrent electrolytic hydrogen and formate productions. *Nat Commun* 10:5335
- Greeley J, Jaramillo TF, Bonde J, Chorkendorff IB, Nørskov JK (2006) Computational high-throughput screening of electrocatalytic materials for hydrogen evolution. *Nat Mater* 5:909–913
- Greeley J, Stephens IEL, Bondarenko AS, Johansson TP, Hansen HA, Jaramillo TF, Rossmeisl J, Chorkendorff I, Nørskov JK (2009) Alloy of platinum and early transition metals as oxygen reduction electrocatalysts. *Nat Chem* 1:552–556
- Zhang M, Dai LM (2012) Carbon nanomaterials as metal-free catalysts in next generation fuel cells. *Nano Energy* 1:514–517
- You B, Liu X, Hu GX, Gul S, Yano J, Jiang DE, Sun YJ (2017) Universal surface engineering of transition metals for superior electrocatalytic hydrogen evolution in neutral water. *J A Chem Soc* 139:12283–12290
- Xie JF, Zhang H, Li S, Wang RX, Sun X, Zhou M, Zhou JF, Lou XW, Xie Y (2013) Defect-rich MoS₂ ultrathin nanosheets with additional active edge sites for enhanced electrocatalytic hydrogen evolution. *Adv Mater* 25:5807–5813
- Ping XF, Liang D, Wu YY, Yan XX, Zhou SX, Hu DK, Pan XQ, Lu PF, Jiao LY (2021) Activating a two-dimensional PtSe₂ basal plane for the hydrogen evolution reaction through the simultaneous generation of atomic vacancies and Pt clusters. *Nano Lett* 21:3857–3863
- Jin HY, Guo CX, Liu X, Liu JL, Vasileff A, Jiao Y, Zheng Y, Qiao SZ (2018) Emerging two-dimensional nanomaterials for electrocatalysis. *Chem Rev* 118:6337–6408
- Zhang X, Luo ZM, Yu P, Cai YQ, Du YH, Wu DX, Gao S, Tan CL, Li Z, Ren MQ, Osipowicz T, Chen SM, Jiang Z, Li J, Huang Y, Yang J, Chen Y, Yen Ang C, Zhao YL, Wang P, Song L, Wu XJ, Liu Z, Borgna A, Zhang H (2018) Lithiation-induced amorphization of Pd₃P₂S₈ for highly efficient hydrogen evolution. *Nat Catal* 1:460–468
- Cai YQ, Gao JF, Chen S, Ke QQ, Zhang G, Zhang YW (2019) Design of phosphorene for hydrogen evolution performance comparable to platinum. *Chem Mater* 31:8948–8956
- Huang HJ, Yan MM, Yang CZ (2019) Graphene nanoarchitectonics: recent advances in graphene-based electrocatalysts for hydrogen evolution reaction. *Ad Mater* 31:1903415
- Gawande MB, Fornasiero P, Zboril R (2020) Carbon-based single-atom catalysts for advanced applications. *ACS Catal* 10:2231–2259
- Fei HL, Dong JC, Chen DL, Hu TD, Duan XD, Shakir I, Huang Y, Duan XF (2019) Single atom electrocatalysts supported on graphene or graphene-like carbons. *Chem Soc Rev* 48:5207–5241
- He XY, Liu F, Lin FT, Shi WZ (2021) Tunable 3D Dirac-semimetals supported mid-IR hybrid plasmonic waveguides. *Opt Lett* 46:472–475
- He XY, Feng Liu F, Lin FT, Shi WZ (2021) Tunable terahertz Dirac semimetal metamaterials. *J Phys D: Appl Phys* 54:235103
- Peng J, He XY, Shi CY, Leng J, Lin FT, Liu F, Zhang H, Shi WZ (2020) Investigation of graphene supported terahertz elliptical metamaterials. *Phys E* 124:114309
- Zhang Y, Xue LX, Liang CB, Chen YZ, Liu JJ, Shen C, Li Q, Duan YF, Yao LY, Zhang H, Cai YQ, Tan CL, Luo ZM (2021) Two-dimensional metallic MoS₂-amorphous CoNi(OH)₂ nanocomposite for enhanced electrochemical water splitting in alkaline solutions. *Appl Surf Sci* 561:150079
- Liu G, Li JJ, Dong C, Wu LY, Liang D, Cao HW, Lu PF (2021) Hydrogen evolution reaction on in-plane platinum and palladium dichalcogenides via single-atom doping. *Int J Hydrogen Energy* 46:18294–18304

26. Huang CC, Li C, Shi G (2012) Graphene based catalysts. *Energy Environ Sci* 5:8848
27. Jia Y, Zhang LZ, Du AJ, Gao GP, Chen J, Yan XC, Brown CL, Yao XD (2016) Defect graphene as a trifunctional catalyst for electrochemical reactions. *Adv Mater* 28:9532–9538
28. Gao XP, Zhou YA, Tan YJ (2019) Single Mo atoms supported on N-doped carbon with N/C edge-site for enhanced electrochemical hydrogen evolution. *Int J Hydrogen Energy* 44:14861–14868
29. Ito Y, Cong WT, Fujita T, Tang Z, Chen MW (2014) High catalytic activity of Nitrogen and Sulfur co-doped nanoporous graphene in the hydrogen evolution reaction. *Angew Chem Int Ed* 54:2131–2136
30. Xue YR, Huang BL, Yi YP, Guo Y, Zuo ZC, Li YG, Jia ZY, Liu HB, Li YL (2018) Anchoring zero valence single atoms of nickel and iron on graphdiyne for hydrogen evolution. *Nat Commun* 9:1460
31. Zhang SH, Zhou J, Wang Q, Chen XS, Kawazoe Y, Jena P (2015) Penta-graphene: a new carbon allotrope. *Proc Natl Acad Sci USA* 112:2372–2377
32. Wang MH, ZhanZY GYQ, Zhou SN, Wang JH, Wang ZJ, Wei SX, Guo WY, Lu XQ (2020) Penta-graphene as a promising controllable CO₂ capture and separation material in an electric field. *Appl Surf Sci* 502:144067
33. Qin HB, Feng C, Luan XH, Yang DG (2018) First-principles investigation of adsorption behaviors of small molecules on penta-graphene. *Nanoscale Res Lett* 13:264
34. Cheng MQ, Chen Q, Yang K, Huang WQ, Hu WY, Huang GF (2019) Penta-graphene as a potential gas sensor for NO_x detection. *Nanoscale Res Lett* 14:306
35. Li B, Shao ZG (2020) Adsorption of DNA/RNA nucleobases and base pairs on penta-graphene from first principles. *Appl Surf Sci* 512:145635
36. Balasubramanian R, Chowdhury S (2015) Recent advances and progress in the development of graphene-based adsorbents for CO₂ capture. *J Mater Chem A* 3:21968–21989
37. Lu XQ, Wang MH, Luo GW, Zhou SN, Wang JH, Xin HL, Wang ZJ, Liu SY, Wei SX (2020) High-efficiency CO₂ capture and separation over N-2 in penta-graphene pores: insights from GCMC and DFT simulations. *J Mater Sci* 55:16603–16611
38. Zhang CP, Li B, Shao ZG (2019) First-principle investigation of CO and CO₂ adsorption on Fe-doped penta-graphene. *Appl Surf Sci* 469:641–646
39. Sathishkumar N, Wu SY, Chen HT (2019) Charge-modulated/electric-field controlled reversible CO₂/H₂ capture and storage on metal-free N-doped penta-graphene. *Chem Eng J* 391:123577
40. Sathishkumar N, Wu SY, Chen HT (2019) Boron-and nitrogen-doped penta-graphene as a promising material for hydrogen storage: a computational study. *Int J Energy Res* 43:4867–4878
41. Xiao B, Li YC, Yu XF, Cheng JB (2016) Penta-graphene: a promising anode material as the Li/Na-ion battery with both extremely high theoretical capacity and fast charge/discharge rate. *ACS Appl Mater Interfaces* 8:35342–35352
42. Wang HW, Luo WW, Tian ZF, Ouyang CY (2019) First principles study of alkali and alkaline earth metal ions adsorption and diffusion on penta-graphene. *Solid State Ion* 342:115062
43. Zheng Y, Jiao Y, Li LH, Xing T, Chen Y, Jaroniec M, Qiao SZ (2014) Toward design of synergistically active carbon-based catalysts for electrocatalytic hydrogen evolution. *ACS Nano* 8:5290–5296
44. Zhang C, Cao Y, Dai X, Ding XY, Chen LL, Li BS, Wang DQ (2020) Ab-Initio study of the electronic and magnetic properties of boron- and nitrogen-doped penta-graphene. *Nanomaterials* 10:816
45. Einollahzadeh H, Fazeli SM (2021) The superconducting transition temperature for P-doped hydrogenated penta-graphene. *Supercond Sci Tech* 34:065003
46. Lu PF (2020) Recent development of two-dimensional stanene. *J Sichuan Normal Univ (Nat Sci)* 43:1–20
47. Manjanath A, Hsu CP, Kawazoe Y (2020) Tuning the electronic and magnetic properties of pentagraphene through the C1 vacancy. *2D Mater* 7:045024
48. Han TW, Wang XY, Zhang XY, Scarpa F, Tang C (2021) Mechanics of pentagraphene with vacancy defects under large amplitude tensile and shear loading. *Nanotechnology* 32:275706
49. Kresse GJ, Furthmuller J (1996) Efficient iterative schemes for ab initio total-energy calculations using a plane-wave basis set. *Phys Rev B* 54:11169–11186
50. Kresse GJ, Joubert D (1999) From ultrasoft pseudopotentials to the projector augmented-wave method. *Phys Rev B* 59:1758–1775
51. Lin S, Liu JC, Li WZ, Wang D, Huang Y, Jia C, Li ZW, Murtaza M, Wang HY, SongJ N, Liu ZL, Huang K, Zu D, Lei M, Hong B, Wu H (2019) A flexible, robust and Gel-free electroencephalogram electrode for noninvasive brain-computer interfaces. *Nano Lett* 19:6853–6861
52. Lin S, Bai XP, Wang HY, Wang HL, Song JN, Huang K, Wang C, Wang N, Li B, Lei M, Wu H (2017) Roll-to-roll production of transparent silver nanofiber network electrode for flexible electrochromic smart windows. *Adv Mater* 29:1703238
53. Perdew J P, Burke K, Ernzerhof M (1996) Generalized gradient approximation made simple. *Phys Rev Lett* 77:3865–3868
54. Monkhorst HJ, Pack JD (1976) Special points for Brillouinzone integrations. *Phys Rev B: Solid State* 13:5188–5192
55. Tang W, Sanville E, Henkelman G (2009) A grid-based Bader analysis algorithm without lattice bias. *J Phys: Condens Matter* 21:084204
56. Henkelman G, Uberuaga BP, Jonsson H (2000) A climbing image nudged elastic band method for finding saddle points and minimum energy paths. *J Chem Phys* 113:9901–9904
57. Guan XN, Zhang R, Jia BN, Wu LY, Zhou B, Fan L, Liu G, Wang Y, Lu PF, Peng GD (2020) Fluorine passivation of ODC defects in amorphous germanium dioxide. *J Non-Cryst Solids* 550:120388
58. Tibbetts K, Miranda CR, Meng YS, Ceder G (2007) An ab Initio study of lithium diffusion in titanium disulfide nanotubes. *Chem Mater* 19:5302–5308
59. Peng B, Cheng FY, Tao ZL, Chen J (2010) Lithium transport at silicon thin film: Barrier for high-rate capability anode. *J Chem Phys* 133:034701
60. Bi K, Yang DQ, Chen J, Wang QM, Wu HY, Lan CW, Yang YP (2019) Experimental demonstration of ultra-large-scale terahertz all-dielectric metamaterials. *Photonics Res* 7:457–463
61. Hinnemann B, Moses PG, Bonde J (2005) Biomimetic hydrogen evolution: MoS₂ nanoparticles as catalyst for hydrogen evolution. *J Am Chem Soc* 127:5308–5309
62. Jiao Y, Zheng Y, Jaroniec MT, Qiao SZ (2015) Design of electrocatalysts for oxygen- and hydrogen-involving energy conversion reactions. *Chem Soc Rev* 44:2060–2086
63. Wei JM, Zhou M, Long AC, Xue YM, Liao HB, We C, Xu ZCJ (2018) Hetero-structured electrocatalysts for hydrogen evolution reaction under alkaline conditions. *Nano-Micro Lett* 10:75

Publisher's Note

Springer Nature remains neutral with regard to jurisdictional claims in published maps and institutional affiliations.